Available online at www.sciencedirect.com

ScienceDirect

Procedia Structural Integrity 54 (2024) 617–625

Structural Integrity Procedia

www.elsevier.com/locate/procedia

International Conference on Structural Integrity 2023 (ICSI 2023)

The role of hydrogen in the corrosion-induced reduction of plane-stress fracture toughness and strain-induced intergranular cracking of AA2024

C.C.E. Pretorius[a,*], R.J. Mostert[a], C-M Charalampidou[b], N. Alexopoulos[b]

[a]*University of Pretoria, Department of Materials Science and Metallurgical Engineering, Lynnwood Road, Hatfield, Pretoria 0002, South Africa.*
[b]*Research Unit of Advanced Materials, Department of Financial Engineering, School of Engineering, University of the Aegean, 41 Kountouriotoustr., 82132Chios, Greece.*

Abstract

The role of diffusible hydrogen in the embrittlement of AA2024 after short-term exposure in the standard exfoliation corrosion (EXCO) test solution (ASTM G34) was investigated. Slow strain rate K_R-curves were established – utilizing the unloading compliance method of the ASTM E561 Standard – on 3.2 mm thick compact tension (C(T)) specimens for the following four (4) sets of samples: (i) as-received (unexposed), (ii) 2 h EXCO exposed, (iii) unexposed and heat-treated, and (iv) 2 h EXCO exposed and heat-treated samples of AA2024. A significant degradation ($\approx 12.0 \pm 1.8$ %) was observed in the effective slow strain rate K_C toughness after short-term exposure of the AA2024-T3 specimens to the EXCO-solution. Post-exposure heat-treatments appear to have restored the plane-stress fracture toughness to its original values. The formation of secondary and primary intergranular cracks in the plastic zone of the C(T) samples were studied using SEM. The presence of intergranular secondary surface cracks in the plastic zones of the C(T) samples was, however, not altered by the heat treatment, and did not appear to influence the fracture toughness results. Thermal desorption mass spectroscopy was exploited to evaluate the extent of hydrogen absorption due to the corrosive exposure, and the effect of the subsequent heat treatment in removing it.

Keywords: Aluminium Alloy 2024; Hydrogen Embrittlement; Plain Stress Fracture Toughness

* Corresponding author. Tel.: +27 76 807 9398
E-mail address: cce.pretorius@gmail.com

10.1016/j.prostr.2024.01.126

1. Introduction

Several studies have shown that the Al-Cu alloys are susceptible to intergranular corrosion. This susceptibility of the alloys to this type of attack has been attributed to the formation of a micro-galvanic coupling (Campestrini et.al (2000)), which arises from the segregation and precipitation of copper-rich constituents at the grain boundaries (Revie (2011)). The precipitation of the copper-rich constituents is also accompanied by the depletion of copper within the surrounding aluminium matrix. As such, chemical heterogeneity exists at these locations, with dissolution occurring at the less noble (copper-depleted) aluminium matrix, e.g. Svenningsen et.al (2006), Lacroix et. al. (2008), Blanc et.al. (2016).

Petroyiannis et.al. (2004) showed that the corrosion-induced degradation of the mechanical properties of the aluminium alloy 2024-T3 cannot solely be attributed to the observed pitting and intergranular corrosion damage. This was concluded after the mechanical removal of the corroded layers, which allowed for a significant restoration in the mechanical strength without restoring the tensile ductility. Petroyiannis et.al. (2004) continued to show that post-exposure heat treatments – after the mechanical removal of the corroded layers – restored the ductility of tensile specimens. Coupled with post-exposure thermal desorption mass spectrometry results, it was concluded that the corrosion of aluminium alloy 2024-T3 is associated with hydrogen embrittlement.

The term – hydrogen embrittlement (HE) – however, limits the acuity of the manner in which the element degrades the material properties (Propov and Djukic (2023)). This is primarily due to the fact that underlying mechanisms of hydrogen embrittlement are not yet fully understood. A variety of models have been proposed to describe the interaction of hydrogen in solution with metallic materials; five of which have found favour due to good correlation with practical results. One of the first models to be proposed, is the so-called stress induced hydride formation and cleavage model (HFV). The model was first proposed by Westlake (1996), with the embrittlement attributed to a repeated sequence of hydride formation and cleavage-like fracture within the plastic zone ahead of a crack tip. Therefore, the model describes hydrogen assisted cracking (HAC) – which refers to the hydrogen-assisted modification of the microscopic processes that constitute the crack tip advance, leading to a degradation in the resistance to crack propagation) – in materials in which hydrides are either stable, or may be stabilized by a stress field (Birnbaum et.al. (1997)). Typically, the group Vb metals, as well as titanium, zirconium and magnesium alloys are considered to be susceptible to this type of hydrogen embrittlement.

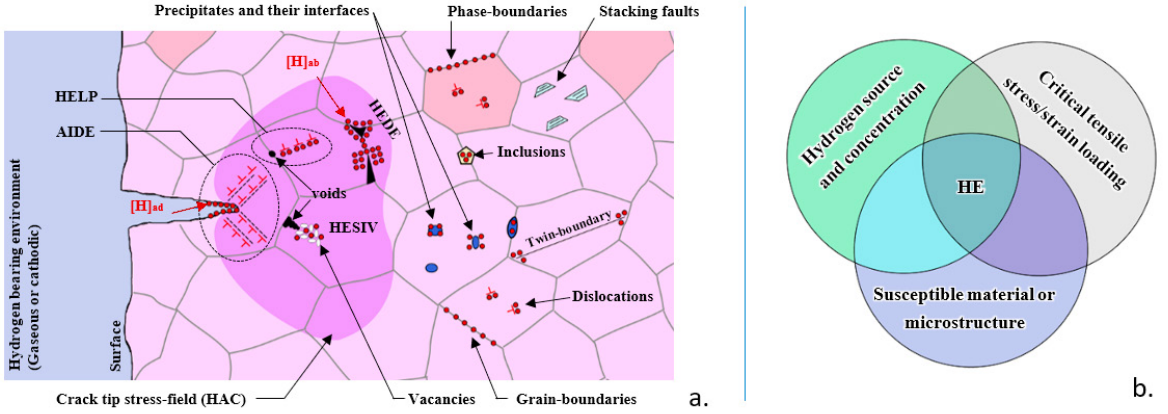

Fig. 1 (a) Schematic representation (adopted from Sun (2023) and Koyama et.al (2017)) of the possible trapping sites for absorbed hydrogen in susceptible metals, as well as the most prominent models of hydrogen embrittlement; note that HAC specifically refers to the modification of the microscopic processes within the crack tip stress-field. (b) Venn diagram showing the three concurrent factors required for the initiation of HE (adopted from Dwivedi and Vishwakarma (2018))

Nomenclature

HE	Hydrogen embrittlement
HAC	Hydrogen assisted cracking
HFV	Stress-induced hydride formation and cleavage
HEDE	Hydrogen enhanced decohesion embrittlement
HELP	Hydrogen enhanced localised plasticity
AIDE	Adsorption induced dislocation emission
HESIV	Hydrogen enhanced strain-induced vacancies
K_R	Crack-extension resistance
K_C	K_R value at maximum applied force
$K_{c,eff}$	K_R value at maximum applied force that does not adhere to the net-stress validity criteria

The remaining four models are summarized in Fig. 1(a), along with discontinuities within the metal matrix that may act as hydrogen trapping sites. In metals where hydrides are not thermodynamically feasible, Troiano (1960,1974) proposed that the presence of hydrogen directly affects the interatomic-bonding strength along grain-boundaries and crystallographic planes; the basis that was later used to develop the Hydrogen Enhanced Decohesion Embrittlement (HEDE) model (Milne et.al. (2003)). The proposed model, therefore, predicts that susceptible metals would show embrittlement on both the macroscopic and microscopic scale during HAC. However, Beachem (1972) showed that the fracture of some hydrogen embrittled steels are accompanied by significant localized plasticity. This led to the development of the hydrogen-enhanced localized plasticity (HELP) model, in which absorbed/dissolved hydrogen is postulated to affect the resistance to dislocation glide and allow for highly localized plastic rupture rather than embrittlement (Milne et.al. (2003)). Lynch (1988) argued that – in the case of Hydrogen Environment Assisted Cracking (HEAC) – hydrogen adsorption at the exposed crack tip is sufficient to initiate the embrittling process. In the proposed model, referred to as Adsorption Induced Dislocation Emission (AIDE) model, adsorbed hydrogen assists in the nucleation and emission of dislocations from the crack tip; with the associated alternating slip facilitating crack tip sharpening and, ultimately, propagation. According to Nagumo and Takai (2019), HE cannot exclusively be ascribed to enhanced dislocation mobility. They showed that dissolved hydrogen may enhance the strain-induced nucleation and clustering of vacancies (HESIV model); thereby assisting in the sequential process of nucleation, growth and linking of voids according to the ductile fracture development.

More recently, a general consensus can be observed in the literature in that HE seldom presents in a single form of the proposed models, but rather that a synergetic interplay exists between these proposed models. The prevailing mechanism of embrittlement depends on the hydrogen charging method, microstructural considerations, the local and global hydrogen distribution, and the applied stress/strain (Djukic et. al. (2019)). Therefore, due to the complex nature of hydrogen-metal interactions, the detailed mechanics of HE still remains a subject to be pursued.

Returning to the aluminium alloy 2024, Pretorius et.al. (2021) reported that the alloy showed a reduction in plane-stress fracture toughness due to corrosion exposure. Additionally, an associated manifestation of intergranular surface cracks within the plastic zone during straining has been reported. The current work specifically focuses on short-term exposure in the standard exfoliation corrosion test (EXCO test, ASTM G34) solution, and investigates the role of hydrogen in the fracture toughness degradation and the formation of the primary and secondary intergranular surface cracking.

2. Materials of consideration

Aluminium alloy 2024-T3 sheet material, with the chemical composition shown in Table 1, was used in the current investigation. Compact tension (C(T)) fracture toughness specimens – with approximate dimensions of 60 mm (W_T) x 57.5 mm (L) x 3.2 mm (B) – were produced from 3.2 mm thick AA2024-T3 sheet material. The envelope of the crack starter notch comprised of a typical straight-through notch that terminated in a narrow-type notch; the latter from which a fatigue starter crack was introduced via cyclic straining in accordance to the ASTM E561 Standard. Additional rectangular samples (approximate dimensions of 38 mm x 8 mm x 3.2 mm) were sectioned from the AA2024-T3 sheet material for the preliminary thermal desorption spectroscopy results.

Table 1 Chemical composition of the AA2024-T3 sheet material compared to the AST B209/B209M specification

		Si	Fe	Cu	Mn	Mg	Cr	Zn	Ti	Al
Aluminium alloy 2024	max	0.50	0.50	4.9	0.9	1.8	0.1	0.25	0.15	rem.
(ASTM B209/B209M)	min	-	-	3.8	0.3	1.2	-	-	-	
Chemical analysis results		0.50	0.50	4.35	0.64	1.50	0.10	0.25	0.15	rem.

3. Aim of the present investigation

If corrosion-induced hydrogen embrittlement is the cause of the fracture toughness degradation and the formation of the intergranular secondary cracking in the plastic zone of the aluminium alloy 2024, then post-exposure heat treatment should, theoretically, be able to reverse these behaviors by the desorption of the absorbed hydrogen. Therefore, the present investigation aims to establish whether a fraction of the material property degradation can be restored by the heat treatments. Additionally, it aims to establish whether the intergranular surface cracking behaviour was altered in any manner after the heat treatment and may be related to a form of hydrogen embrittlement.

4. Experimental procedure

Slow strain rate crack-extension resistance (K_R) curves were established utilizing the unloading compliance method as described in the ASTM E561 Standard on 3.2 mm thick C(T)-(L-T) specimens. A set of reference tests (designated as AA2024-T3 UE in Table 2) were performed on samples prior to any exposure in order to attain the baseline plain-stress fracture toughness results. An additional set of tests was performed in order to establish the effect of the heat treatment on the fracture toughness (designated by AA2024-HT samples). The heat treatment comprised of a T62 temper as described in the ASTM B918/B918M Standard, with an extended solution heat treatment soaking time of 2 hours.

The remaining K_R tests may be divided into EXCO exposed (designated by AA2024-T3 EE) and EXCO exposed and heat treated (designated by AA2024-T3 EE/HT) specimens. Prior to the exposure procedure, most of the external surface of the specimens was shielded off using PVC tape to limit the exposure to an area near and ahead of the notch/pre-crack configuration. The specimens were cleaned in ethanol and exposed to the standard EXCO test solution (ASTM G34 Standard) for two (2) hours. The shielding was then removed and the specimens were washed in acetone for approximately 5 minutes. Slow strain-rate K_R-curves were established immediately after the exposure procedure of the AA2024-T3 EE specimens, whereas the AA2024-T3 EE/HT specimens were first subjected to the heat treatment procedure. The K_R-tests were established at a constant crosshead displacement rate of 0.03 mm/min.

The formation of secondary (on the specimen surface and parallel to the primary crack-plane) and primary intergranular cracks in the plastic zone of the C(T) samples were studied using a Zeiss 540 Cross-beam FEG SEM at an excitation voltage of 20 kV. Thermal desorption mass spectroscopy was utilized to evaluate the extent of hydrogen absorption by comparing the different investigated material conditions. The square samples (mentioned in section 2) were subjected to the relevant exposure conditions and cleaned in acetone (10 min). Thereafter, the hydrogen desorption was analyzed using the Bruker G4 Phoenix which was set to ramp the temperature from ambient to 495 ºC at a constant ramp rate of 10 ºC/min, followed by soaking at 495 ºC for 20 min.

5. Results and discussion

5.1. Comparison of the K_c and TDS results

The effective K_c values for the different exposure conditions are summarized in Table 2. It is clear from the results that fairly large K_c values were established for all of the material conditions using the given C(T) specimen geometry and size. The net section stress validity criterion states that valid K_R-values are only valid if the uncracked ligament of material remains primarily elastic. For the current tests, significant plasticity is indicated for the remaining ligament of material due to the size of the selected C(T)-specimens and the non-standard slow strain-rate test procedure. It is, however, argued that the increased size of the plastic-zone may assist in the detection of embrittlement in the form of

hydrogen assisted cracking. That is, since hydrogen modifies the microscopic processes that constitute crack tip advance, detection of the embrittlement should be facilitated when using specimens that originally have the ability to absorb the applied energy through plastic response. Therefore, the current results are not considered to yield accurate K_c values, but rather aid as a comparative tool to establish whether embrittlement has occurred. It is for these reasons that the values are referred to as $K_{c,eff}$ values.

Table 2. The effective slow strain-rate K_C values for the different exposure conditions as established via the unloading compliance method of the ASTM E561 Standard.

Condition of the investigated specimens	Reference specimens	Heat-treated specimens	EXCO exposed specimens	EXCO exposed and heat-treated specimens
Code name	AA2024 -T3 UE	AA2024-T3 HT	AA2024-T3 EE	AA2024-T3 EE/HT
$K_{c,eff}$ (MPa·√m)	131±2	126 ± 2	115 ± 2	131 ± 4

Fig. 2 compares the $K_{c,eff}$ values in terms of the fraction of original toughness (equation 1) and fractional loss in toughness (equation 2) using AA2024-T3 UE as the reference specimen. A very minor decrease ($F_{loss} \approx$ - 3.4 ±1.2 %) could be observed in the $K_{c,eff}$ value after purely performing the heat treatment on the 2024-T3 alloy. The 2h-EXCO exposed samples, however, revealed a significant degradation in the $K_{c,eff}$ value of approximately 12.0 ± 1.7 %; which was found to be comparable to the 11.2 % loss earlier reported by Pretorius et.al. (2021). Finally, the post-exposure heat-treatment appears to have restored the $K_{c,eff}$ values when compared to the AA2024-T3 UE specimens.

$$F_{K_c} = \frac{K_{c,i}}{K_{c,AA2024-T3\ UE}} \tag{1}$$

$$F_{loss} = \frac{K_{c,i} - K_{c,AA2024-T3\ UE}}{K_{c,AA2024-T3\ UE}} \tag{2}$$

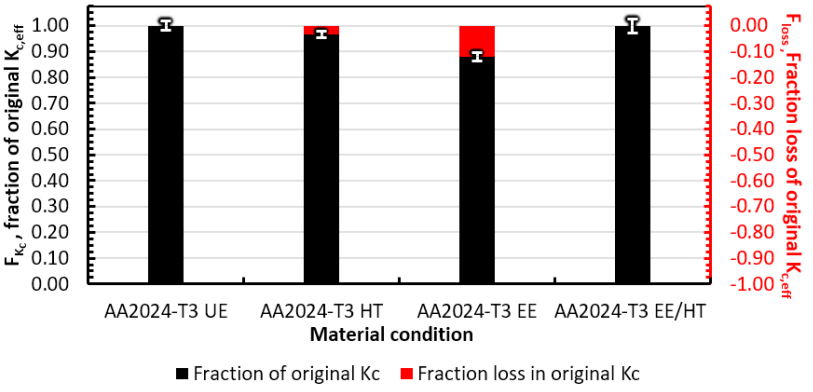

Fig. 2 Comparison of the K_{Rc_eff} test results according to the fraction of original toughness and fractional loss in toughness.

The K_c results, therefore, imply that the crack-growth resistance behaviour of AA2024 has been degraded due to corrosion induced hydrogen embrittlement. If this is the case, the TDS results are expected to reveal a higher hydrogen concentration when compared to the as received material. The overall hydrogen content according to the TDS analysis is summarised in Table 3. It is clear that the unexposed specimen revealed the lowest hydrogen concentration. From the hydrogen desorption-rate curve (TDS-profile) in Fig. 3, it appears that most of the hydrogen was liberated at temperatures in excess of 410 ºC. Considering the work by Kamoutsi et.al. (2006), this may be attributed to the release of hydrogen from trapping sites T3 and T4. Trapping site T3 (410 ºC) has been attributed to the formation of magnesium hydride, whilst T4 (solution temperature range) has been attributed to the dissolution of the

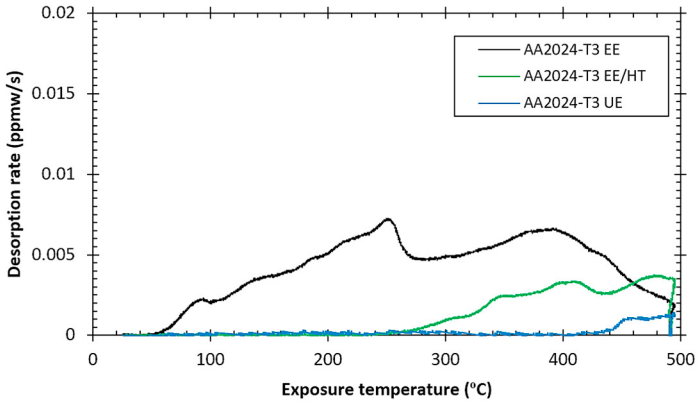

Fig. 3 TDS profiles for the various exposure condition of the aluminium alloy 2024-T3 (ramp-rate of 10ºC/min)

Table 3 Hydrogen content in the various exposure conditions as determined via TDS analysis at a heating rate of 10ºC/min

Exposure condition	AA2024 -T3 UE	AA2024-T3 EE	AA2024-T3 EE/HT
Hydrogen content (ppmw)	0.8	12.1	3.9

strengthening phase. Successful separation of the TDS-peaks was, however, not fully achieved due to the fairly rapid ramp-rate of 10 ºC/min. Nevertheless, a clear difference can be seen in the results when considering the different exposure conditions. The AA2024-T3 EE sample showed nearly continuous desorption throughout the ramping temperature range, indicating that both reversible (T1) and irreversible (T2 through T4) hydrogen trapping sites are active. However, the post-exposure heat treatment appears to have allowed for the desorption of hydrogen from the reversible traps (lower temperature range), with hydrogen desorption only observed at temperatures in excess of the T2 trapping site (210 ºC). This latter trapping site is associated with the incoherent interfaces of dispersoids and the loss in coherency of the strengthening phases (Kamoutsi et.al. (2006)).

The observation that the AA2024-T3 EE releases hydrogen from reversible traps is revealing when considering the fracture toughness results. This is due to the ability of reversible hydrogen traps to continuously supply hydrogen to assist in the modification of the microscopic processes at the crack tip. Therefore, the TDS-results show good agreement with the $K_{c,eff}$ results. Slower ramp-rates are, however, required in order to establish the active trapping sites after 2 hours of corrosion exposure, and avoid overlapping of the TDS peaks.

5.2. Primary crack fracture morphology and secondary intergranular cracking of EXCO exposed AA2024-T3

Fig. 4 summarizes the fractography results along the primary crack for the various exposure conditions. Concerning the crack produced during the slow strain-rate K_R-testing, the bulk of the material showed ductile crack propagation regardless of the exposure procedure. In accordance to the results by Pretorius et.al (2021), the primary crack extension comprises of a triangular region of stable (ductile) crack extension, with the surrounding fracture morphology comprising of a ductile shear fracture. The crack plane of the former region was oriented roughly 90º to the principal applied stress, whilst the remaining fracture morphology was orientated at 45º. SEM fractography revealed microvoids (MV) within both the stable-crack extension and 45º shear regions for the bulk of the material (refer to Fig 4(b) through (d)). However, whereas this ductile behaviour extends to the external surface of the AA2024-T3 UE specimens, a transition towards a shallow layer (up to 146 µm in depth) of intergranular cracking is seen for both the AA2024-T3 EE and AA2024-T3 EE/HT specimens (represented by Fig 4(e)) near the exposed surfaces. The current SEM investigations revealed fine microvoids (represented by Fig. 4(d)) directly adjacent to the intergranular cracking region for both the AA2023-T3 EE and EE/HT specimens. However, further SEM studies are proposed in order to establish whether any quasi-cleavage type fracture behaviour is detectable; especially for the AA2024-T3 EE sample.

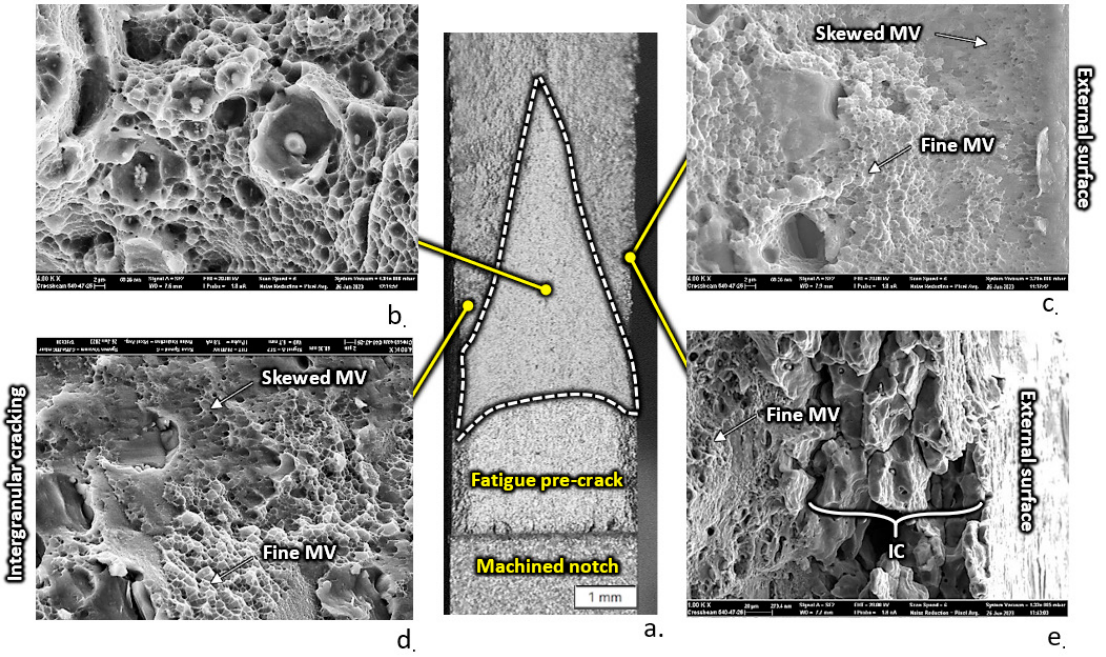

Fig. 4 Typical fracture morphologies as observed on the primary crack front; (a) an overview stereo-micrograph showing the typical bulk crack-extension behaviour, with the remaining SEM images showing (b) the microvoid coalescence within the triangular stable crack extension region of (a), observable in all exposure conditions, (c) the fracture morphology near the external fracture surface of the unexposed material, showing with fine and skewed microvoids are observable up to the external surface, (d) the fine and skewed microvoids observable just adjacent to the (c) the intergranular cracking observed near the external exposed surface EXCO exposed specimens. **Nominal magnifications:** (a) 8X, (b) through (d) 4000X, (e) 1000X

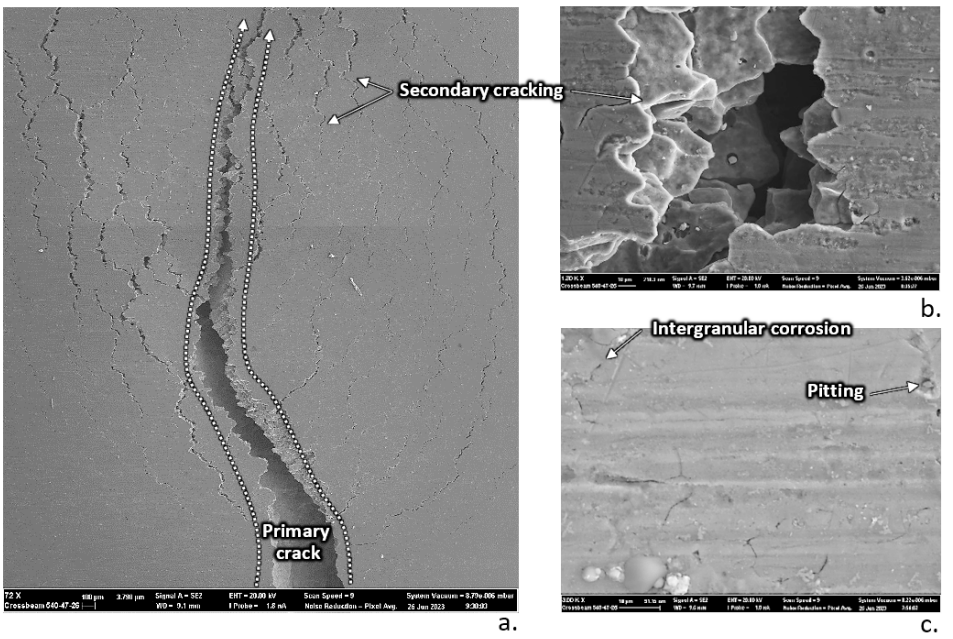

Fig. 5 SEM micrographs summarising the condition of the exposed surface perpendicular to the primary crack front after K_R-testing of the AA2024-T3 EE and EE/HT specimens; (a) overview micrograph showing the secondary surface cracks within the plastic zone adjacent to the primary crack front, (b) showing the intergranular nature of the secondary cracks, and (c) the corrosion damage observed on the exposed surface ahead of the plastic zone.

Secondary intergranular cracks (Fig. 5(a) and (b)) were also observed within the plastic zone of the EXCO-exposed materials. Similar to the intergranular fracture observed on the primary crack front, the secondary cracking was found to persist after the post-exposure heat treatment (Fig. 5(a)). It is, therefore, reasonable to conclude that the layer of embrittled material near the exposure surface likely resulted from the well-documented mechanism of intergranular corrosion, rather than the HEDE mechanism. This appears to be supported by the SEM fractographs taken at locations outside of the plastic zone of the specimens (Fig 5(c)), where the secondary cracking was no longer observed. Indications of corrosion, in the form of intergranular and pitting (white arrowed) corrosion, could be observed at these locations. It is, however, clear from the $K_{c,eff}$ results that this embrittled layer of material did not have a significant effect the on the $K_{c,eff}$-values.

6. Conclusions

- Short-term EXCO exposure leads to a significant reduction of crack growth resistance and critical crack growth resistance, as expressed in $K_{c,eff}$ -values for the AA 2024T3 alloy investigated.
- A solution and ageing heat treatment fully restores the crack growth resistance and $K_{c,eff}$ -values.
- The plane stress toughness reduction referred to above is due to hydrogen embrittlement, as shown through TDS testing.
- The surface intergranular cracking (primary and secondary) observed after short-term EXCO exposure and K_R-testing was not influenced by the post-exposure heat treatment. This leads to the conclusion that the layer was not a result of diffusible hydrogen embrittlement, but rather due to intergranular corrosion.
- The bulk of fracture surface showed microvoid coalescence for all material conditions considered, indicating that the mechanism of hydrogen embrittlement associated with the AA2024-T3 EE alloys must one that enhances plasticity (HELP, AIDE or HESIV). Further SEM studies are proposed in order to establish whether any quasi-cleavage type fracture behaviour is detectable.
- The surface intergranular cracking (primary and secondary) does not appear to contribute to the degradation in $K_{c,eff}$ for the selected C(T) specimen geometry.

Acknowledgements

The financial funding from the Light Metals Development Network (LMDN) forming part of DSI is greatly acknowledged.

References

Beachem, D., 1972. A new Model for Hydrogen-Assisted Cracking (Hydrogen Embrittlement). Metall. Trans. 3, pp. 437-451.

Birnbaum, H., Robertson, I., Sofronis, P. & Teter, D., 1997. Mechanisms of Hydrogens Related fracture – A Review. In: Magnin T. (ed.) Corrosion-Deformation Interactions CDI '96: (EFC 21). London: Instutute of Materials, pp 128-195.

Blanc, C., Freulon, A., Lafont, M.C., Kihn, Y., Mankowski, G., 2016. Modelling the corrosion behaviour of Al2CuMg coarse particles in copper-rich aluminium alloys. Corrosion Science 48, 3838-3851.

Campestrini, P., van Westing, E.P., van Rooijen, H.W., de Wit, J.H., 2000. Relation between microstructural aspects of AA2024 and its corrosion behaviour investigated using AFM scanning potential technique. Corrosion Science 48, 1853-1861 (2000)

Djukic, M.B., Bakic, G.M., Zeravcic, V.S., Sedmak, A., Rajicic, B., 2019. The synergistic action and interplay of hydrogen embrittlement mechanisms in steels and iron: Localised plasticity and decohetion. Engineering Fracture Mechanics 216, 1-33.

Dwivedi, S.K., Vishwakarma, M., 2018. Hydrogen Embrittlement in different materials: A review. International Journal of Hydrogen Energy 43, 21603-21616.

Kamoutsi, H., Haidemenopoulos, G.N., Bontozoglou, V., Pantelakis, S., 2006. Corrosion-induced hydrogen embrittlement in aluminium alloy 2024. Corrosion Science 48, 1209-1224.

Koyama, M., Rohwerder, M, Tasan, C.C., Bashir, A., Akiyam, E., Takai, K., Raabe, D., Tsuzaki, K., 2017. Recent progress in microstructura hydrogen mapping in steels: quantification, kinetic analysis, and multi-scale characterization. Materials Science and Technology 33, 1481-1496.

Lacroix, L., Ressier, L., Blanc, C., Mankowski, G., Combination of AFM, SKFM, and SIMS to study the corrosion behaviour of S-phase particles in AA2024-T351. Journal of the Electrochemical Society 155, C131-C137.

Lynch, S., 1988. Environmentally assisted cracking: Overview of evidence for an adsorption-induced localised-slip Process. Acta Metallurgica 20, pp. 2639-2661.

Milne, I., Ritchie, R. & Karihaloo,B., 2003. 6.02.7.2 Hydrogen Assisted Damage mechanisms. In: Comprehensive Structural Integrity, Volumes 1-10. Elsevier, pp.69-74.

Nagamu, M., Takai, K., 2019. The predominant role of strain-induced vacancies in hydrogen embrittlement of steels: Overview. Acta Materialia 165, 722-733.

Petroyiannis, P.V., Kermanidis, Al.Th., Papanikos, P., Pantelakis, Sp.G., 2004. Corrosion-induced hydrogen embrittlement of 2024 and 6013 aluminium alloys. Theoretical and Applied Fracture Mechanics 41, 173-183.

Pretorius, C.C., Mostert, R.J., Ramjee, S., 2021. The crack growth resistance behaviour of aluminium alloy 2024-T3 at slow strain rates after exposure to standard corrosive environments. Journal of the Southern African Institute of Mining and Metallurgy 121, 151-158

Propov, B.N., Djukic M.B., 2023. Hydrogen embrittlement theory and prevention of H damage in metals and Alloys. 1st Edition, Elsevier Science.

Revie, R., 2011. Uhlig's Corrosion Handbook (3rd Edition), John Wiley & Sons, pp. 762-740

Sun, B., 2023. Hydrogen Embrittlement in High-Performance Alloys, Max-Plank-Institut, Available at: https://www.mpie.de/4604692/hydrogen_embrittlement (accessed on 15 September 2023)

Svenningsen, G., Larsen, M.H., Walmsley, J.C., Nordlien, J.H., Niscancioglu, K., 2006. Effect of thermomechanical history on intergranular corrosion of extruded AlMgSi(Cu) model alloy. Corrosion Science 48, 3969-3987 (2006)

Svenningsen, G., Lein, J.E., Bjorgum, A., Nordlien, J.H., Yu, Y.D., Nisancioglu, K., 2006. Effect of high temperature heat treatment on intergranular corrosion of AlMgSi(Cu) model alloy. Corrosion Science 48, 258-272

Troiano, A., 1960. The role of hydrogen and other interstitials in the mechanical behavior of metals, Trans. ASM 52, 54-80

Westlake, D., 1969, Generalised model for hydrogen embrittlement. Trans. ASM 62, 1000-1006.